Supporting information

Narcissistic Self-Sorting of *n*-Acene Nano-Ribbons yielding Energy-Transfer and Electroluminescence at p-n Junctions

*Philip Schäfer,[a] Christiaan de Vet,[a] Leire Gartzia-Rivero,[a,b] Guillaume Raffy,[a] Min-Tzu Kao,[a] Christian Schäfer,[a] Laura J. Romasanta,[c] Bertrand Pavageau,[c] Yu-Tang Tsai,[a,d] Lionel Hirsch,[d] Dario M. Bassani,[a] André Del Guerzo[a]**

I. Materials and methods

Unless otherwise stated, all reagents and chemicals were commercially available and used as received. Anhydrous THF or DCM were obtained by distilling it over sodium/benzophenone or CaH_2, respectively. Anhydrous DMSO, MeOH, DMF were purchased from Acros Chemicals containing an AcroSeal® and 4 Å molecular sieves. For all moisture sensitive reactions, the used glassware was dried in the oven overnight prior to the reaction. K_2CO_3 was kept stored in the oven.

Column chromatography was performed on Sigma Aldrich Silica 40 (230-400 mesh size or 40-63 μm) as stationary phase. Thin layer chromatography was performed on TLC Silica gel 60 F254 coated aluminium plates from Merck.

^{1}H-NMR and ^{13}C-NMR-spectra were recorded on a Bruker Avance I300 (^{1}H: 300 MHz, ^{13}C: 75 MHz) or a Bruker Avance III 600 (^{1}H: 600 MHz, ^{13}C: 150 MHz) and chemical shifts (δ) are reported in parts per million (ppm) referenced to tetramethylsilane (^{1}H) or the internal solvent signal (^{13}C). Coupling constants were reported in Hz. The multiplicity of the shifts are given as s = singlet, d = doublet, t = triplet, q = quintet, m = multiplet.

Mass spectra were ran using an ESI-QTOF mass spectra (including all HRMS) performed on a QStar mass spectrometer of Applied Biosystems equipped with an ESI source and a time of flight detector.

II. Synthesis

The 2,3-dimethoxy-6,11-diphenyltetracene-5,12-dione[1] and 2,3-didecyloxyanthracene[2] were synthesized as previously described.

2,3-bis(decyloxy)-6,11-diphenyltetracene-5,12-dione

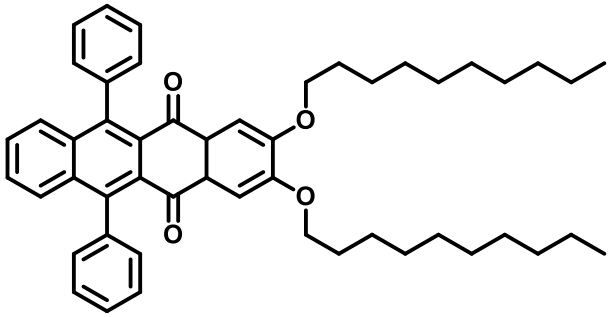

To a solution of 2,3-dimethoxy-6,11-diphenyltetracene-5,12-dione (300 mg, 0.65 mmol) in *dry* CH_2Cl_2 (20 mL) BBr_3 (1 M in CH_2Cl_2, 1.56 mL) was added dropwise at 0°C under argon while stirring vigorously. After 30 min, the ice bad was removed and the reaction was left to come to room temperature. After 2 hours, the reaction was refluxed at 60°C for 1 hour.

The reaction was cooled down to room temperature and given in H_2O with a bit of HCl and extracted with Et_2O (3x). The collected organic fractions were washed subsequently with H_2O (2x) and brine (1x), dried over $MgSO_4$ and concentrated *in vacuo*.

The crude product was dissolved in dry DMF (20 mL) under argon and K_2CO_3 (392 mg) as added to the solution and stirred at room temperature. After 45 min, 1-bromodecane (0.38 mL) was added and the reaction was heated till 135°C overnight. Solvents were evaporated *in vacuo* and the crude product was purified by column chromatography using CH_2Cl_2: petroleum ether (40:60) and was precipitated with DCM/MeOH to obtain a yellow solid (170 mg, 0.24 mmol, 36%) MS [FD+]: m/z 754.42, 1467.85. HRMS [FD+]: m/z calcd for $C_{50}H_{58}O_4Na$ 745.4227 found 745.4215. ^{1}H-NMR (300 MHz, $CDCl_3$): δ 7.64-7.42 (m, 12H, ArH), 7.34-7.28 (m, 4H, ArH), 4.04 (t, ^3J = 6.7 Hz, 4H, OCH_2), 1.82 (q, 4H, OCH_2CH_2), 1.5-1.15 (m, 28, CH_2), 0.88 (t, ^3J = 6.9 Hz, 6H, CH_3). ^{13}C-NMR (75 MHz, $CDCl_3$): δ 183.38; 153.72; 143.84; 140.93; 135.76; 129.57; 128.85; 128.76; 128.64; 128.47; 127.62; 127.06; 109.07; 69.45; 32.04; 29.69; 29.47; 28.98; 25.98; 22.82; 14.27.

2,3-bis(decyloxy)-6,11-diphenyl-5,12-bis(phenylethynyl)tetracene

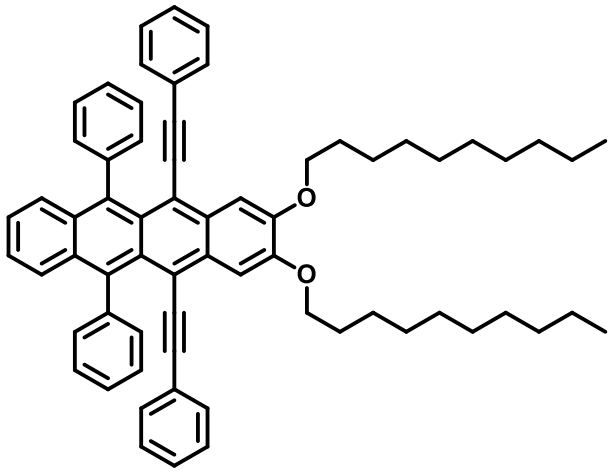

To a solution of phenylacetylene (0.08 mL, 0.69 mmol) in dry THF (5 mL) *n*-BuLi (0.42 mL, 1.6 M in hexane) was added dropwise while stirring vigorously at -78°C under argon. 2,3-bis(decyloxy)-6,11-diphenyltetracene-5,12-dione (100 mg, 0.14 mmol) was dissolved in dry THF (5 mL) and after 30 min dropwise added to the reaction mixture at -78°C. After additional 45 min the acetone bath was removed and the reaction was allowed to reach room temperature. After 4 hours, the solution was quenched with a saturated NH_4Cl solution and extracted in Et_2O. The collected organic fractions were washed with H_2O (2x) and brine (1x), dried over $MgSO_4$ and concentrated *in vacuo*. The crude was dissolved in Et_2O (7 mL) followed by $SnCl_2$ (80 mg, 0.639 mmol) in 10% HCl solution (5 mL) under argon. The reaction was protected from light and refluxed at 60°C for 30 min. Afterwards the reaction was allowed to cool down to room temperature for 1 hour. The reaction was given in H_2O and extracted with Et_2O several times. The organic fractions were collected and washed with H_2O (2x) and brine (1x), dried over $MgSO_4$ and concentrated *in vacuo*. The crude product was purified by column chromatography using CH_2Cl_2:petroleum ether (25:75) and recrystallized from DCM/MeOH to give a purple solid (18 mg, 0.02 mmol, 14%). MS [EI] m/z: 859.52; 1786.2. HRMS: m/z calcd for $C_{66}H_{68}O_2$ 892.52193 found 892.5253. ^{1}H-NMR (400 MHz, $CDCl_3$): δ 7.83 (s, 2H, ArH), 7.61-7.57 (m, 4H, ArH), 7.57-7.54 (m_c, N = 10 Hz, 2H, ArH), 7.5 (t, J = 7.4 Hz, 4H, ArH), 7.38-7.32 (m, 2H, ArH), 7.28 (s, 10H, ArH), 7.25-7.21 (m_c, N = 10 Hz, 2H, ArH), 4.14 (t, J = 6.8 Hz, 4H, OCH_2), 1.89 (q, 4H, CH_2), 1.45 (q, 4H, CH_2), 1.35-1.2 (m, 24H, CH_2), 0.88 (t, J = 6.8 Hz, 6H, CH_3). ^{13}C-NMR (100 MHz, $CDCl_3$): δ 151.47, 141.56, 137.18, 132.79, 132.31, 131.63, 130.65, 128.14, 128.00, 127.83, 127.59, 127.01, 125.21, 124.38, 115.96, 107.68, 105.20, 90.37, 68.92, 32.07, 29.78, 29.71, 29.51, 28.92, 26.14, 22.85, 14.28.

9,10-dibromo-2,3-bis(decyloxy)anthracene

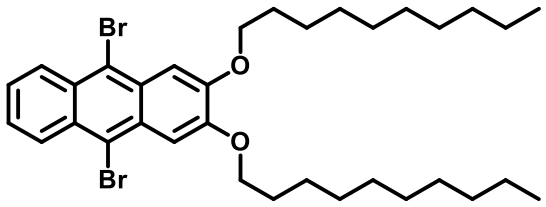

To a solution of 2,3-didecyloxyanthracene (0.72 g, 1.47 mmol) in DCM (120 mL) tetra-*n*-butylammonium-tribromide (TBATB, 1.56 g, 3.23 mmol) was added under argon. After stirring for 5 hr at room temperature, the mixture was concentrated *in vacuo*. The crude product was purified by column chromatography using CH_2Cl_2:petroleum ether (1:4) to give a greenish solid (0.89 g, 1.37 mmol, 93%). ^{1}H-NMR (300 MHz, $CDCl_3$): δ 8.45 (m_c, N = 10 Hz, 2 H, ArH), 7.70 (s, 2 H, ArH), 7.52 (m_c, N = 10 Hz, 2 H, ArH), 4.21 (t, ^3J = 6.6 Hz, 4 H, OCH_2), 1.95 (q, 4 H, CH_2), 1.55 (m, 4 H, CH_2), 1.20-1.46 (m, 24 H, CH_2), 0.87 (t, ^3J = 6.7 Hz, 6 H, CH_3). ^{13}C-NMR (75 MHz, $CDCl_3$): δ), 151.48, 129.82, 128.02, 127.74, 126.31, 120.48, 106.17, 68.95, 31.93, 29.65, 29.59, 29.43, 29.37, 28.90, 26.10, 22.69, 14.11.

2,3-bis(decyloxy)anthracene-9,10-dicarbonitrile

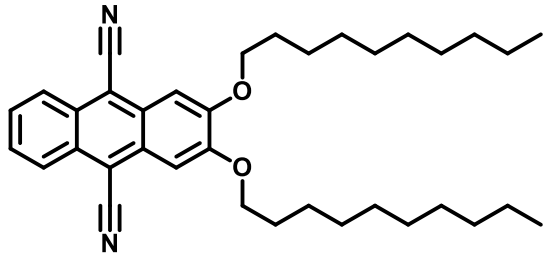

To a solution of 2,3-bis(decyloxy)-9,10-dibromoanthracene (0.15 g, 0.23 mmol) in DMF (10 mL) CuCN (50 mg, 0.56 mmol) was added under argon. After 72 hr of reflux (170°C), the mixture was cooled to room temperature and ethylene diamide (20 mL) and H_2O (60 mL) were added. After the addition, the mixture was extracted with Et_2O. The combined organic fractions were washed with H_2O (2X), brine (1x), dried over $MgSO_4$ and concentrated *in vacuo*. The crude product was purified by column chromatography using CH_2Cl_2:petroleum ether (1:2) to give a yellow solid (95 mg, 0.17 mmol, 76%). HRMS [EI] calcd for $C_{36}H_{48}O_2N_2$ 540.78, found m/z = 540.12 [M+]. ^{1}H-NMR (300 MHz, $CDCl_3$): δ 8.32 (m_c, 2H, ArH), 7.69 (m_c, 2H, ArH), 7.46 (s,

2H, ArH), 4.21 (t, J = 6.5 Hz, 4H, OCH_2), 1.95 (m, 4H, CH_2), 1.55 (q, 4H, CH_2), 1.20-1.47 (m, 24H, CH_2), 0.88 (t, J = 6.5 Hz, 6H, CH_3). ^{13}C-NMR (100 MHz, $CDCl_3$): δ 153.39, 130.24, 130.22, 128.30, 125.42, 116.51, 107.72, 103.04, 69.35, 31.91, 29.62, 29.57, 29.38, 29.35, 28.80, 26.01, 22.68, 14.10.

III. Experimental section

a. Optical Spectroscopy

UV/vis absorption spectroscopy was performed on a Varian Cary 5000. Fluorescence spectra were recorded with a Horiba JobinYvon Fluorolog spectrofluorimeter in right-angle configuration. A Labsphere optical Spectralon Integrating sphere (diameter 100 mm) was used to measure quantum yields and to take absorption spectra for the solid state samples in synchronous mode, correcting the spectra with a graphite suspension as reference.

b. Fluorescence Microscopy

The confocal fluorescence microscopy (CFM) was realized on a Picoquant Microtime 200 inverted confocal microscope using a multichannel single photon counter, two SPAD detectors (MPD) and a Picoquant 375 nm diode laser to carry out fluorescence lifetime imaging (FLIM) and polarization microscopy. The "vertically" polarized laser beam was coupled to a polarization maintaining single-mode fiber optic, collimated and finally injected by 90° reflection on a 80%T/20%R spectrally flat beam splitter into the microscope oil immersion objective (Olympus 100× UPLSAPO, N.A. 1.4). The emission was collected through the same objective, transmitted through the beam splitter and a 405 nm long-pass interferential filter and subsequently focused on a 50 µm pinhole. Parallel and perpendicular components of the emitted light were split by a polarizing beam splitter and polarization cleaned applying two Glan-Thompson polarizers. Due to wavelength dependence of the detectors the G-factor was measured for several narrow spectral regions applying bandpass filters (455 - 480 nm, 510 - 550 nm, 608 - 650 nm) and a 720 longpass filter on a white emissive dilute dye solution. The G-factor is then given by the relation $G = I_{//}/I_{\perp}$, where $I_{//}$ and $I_{\perp}$ are the intensities of the components of the fluorescence emission parallel and perpendicular, respectively, to the polarization of the excitation beam. The polarization P of each pixel is given by $P = (I_{//} - G \times I_{\perp})/(I_{//} + G \times I_{\perp})$. By choosing ROIs (regions of interest), individual ribbons' emission polarization could be analyzed. A similar procedure was used for the

polarization and the fluorescence lifetime measurements: in those cases a distribution of P values or lifetime values of the ROI was analysed, and the center of distribution reported in the manuscript as being the polarization or the lifetime, respectively. For fluorescence hyperspectral imaging, the same microscope and laser were used, but the emission light was diverted after the pinhole into an Andor SR300i spectrometer equipped with a Newton EMCCD. With a 6 ms/pixel scan a high resolution spectrum was taken for each pixel and then converted into CIE coordinates and RGB-colors. The emission spectrum of a selected ROI could be obtained by accumulating spectra of the pixels within the ROI selected *via* the hyperspectral image. The emission spectra were intensity corrected by using an ARGOLIGHT calibration slide.

The independent growth of the ribbons was followed by video-microscopy. Exciting both compounds in epi-illumination with a SOLIS LED (385 nm) through the oil immersion objective (100 × UPLSAPO, N.A. 1.4) and live fluorescence imaging was accomplished through the same objective. In the image plane, a slit was applied to reduce the field of view in x. After collimation of the beam, a 50/50 beam-splitter in 90° configuration creates two images which are recombined by a slightly tilted second mirror and a focusing lens onto two halves of a CCD-camera. The angle between the two beams was kept small by placing the beam-splitter and the mirror in close proximity. To follow the growth of **n-BG** and **p-R**-ribbons separately, a bandpass (510 - 550 nm) and a 720 longpass filter were inserted in the respective paths. The filters were chosen in a way that the background stemming from dissolved dyes was minimized, and the red-shifted emission of the aggregates was favored.

c. Cyclic voltammetry

Cyclic voltammetry (CV) experiments were conducted with an Autolab PGSTAT302N potentiostat. The electrode surface was polished with alumina-water slurry before use. Solutions were degassed by argon bubbling prior to measurements. Experiments were performed in distilled dichloromethane with tetrabutylammonium hexafluorophosphate as supporting electrolyte. Redox potentials were referenced internally against ferrocenium/ferrocene (Fc+/Fc).

d. General sample preparations

The nanoribbons samples were prepared as follows.

Method 1 (thermal treatment): This method was used for the **mixed ribbons** experiments. First, the compounds (2 mM of both **n-BG** and **p-R**) are mixed with the solvent (1 ml of n-butanol or DMSO, or mixture thereof) at room temperature. The mixture was then heated to least at 80°C in the dark with continuous N_2 purging, briefly until a clear solution is obtained. Finally, the solution is left at room temperature (22°C) to allow it to cool down, and kept in the dark and under anoxia until the measurements are performed (usually for several hours, except for measurements of growth by video-microscopy).

Method 2 (injection method): Pristine nanoribbons of **n-BG** were prepared by injecting 100 μL of a 2 mM dichloromethane solution into the same volume of *n*-butanol. Settling of nanoribbons did not occur.

Microscopy studies: To perform microscopy, first a small amount of dispersion of nanoribbons in solvent is taken with a glass pipette (a small sonication of the test-tube may be necessary to disperse the ribbons, but is usually avoided). A few drops of the dispersion are then dropped from a small height onto a rotating (200 – 1000 rpm) standard microscopy glass coverslip mounted on a spin-coater (for about 30 seconds). The solvent evaporates quickly, and the samples are transferred to an air-tight sample holder and placed under gentle N_2 flow to prevent from water condensation. When DMSO is used, the samples are immediately transferred from the spin-coater to a vacuum-chamber and dried under vacuum in the dark for several hours before the study.

For electroluminescence experiments, the nanoribbon dispersions are spincoated onto the PEDOT:PSS layer and immediately put into a vacuum for a day to evaporate any residual solvent. The PEDOT:PSS (ClevosTM PH 1000) is purchased from Heraeus with a ratio of 1:2.5 by weight and a solid content of 1.0 – 1.3% in water. Prior to the spin-coating process, PEDOT:PSS is sonicated for one hour at room temperature, and then filtered with a polyvinylidene fluoride membrane filter with pore diameter of 450 nm to extract bigger aggregates. The solution is spincoated (12.5 microL/cm^2) on clean and plasma treated glass surfaces for 60 s at 1000 rpm. After annealing at 120°C for 15 min and soft plasma treatment, the resulting film has a height of about 40 nm. A solvent post-treatment is performed by covering the

electrode with ethylene-glycol and incubating for 10 minutes. After removal of the solvent, the sample is annealed for 15 min at 120°C. The same procedure is repeated with a distilled water treatment. The electron transport layer TBPi is thermally evaporated under vacuum at a low deposition rate of 0.3 Angström s^{-1}. The deposition thickness (100 nm) is monitored using a thickness monitor inside the vacuum chamber close to the substrate holder. Thicknesses are checked with a Tencor AS-IQ profilometer. Bilayer cathodes of lithium fluoride (LiF, 1 nm thick) and aluminum (Al, 120 nm thick) are then evaporated through a shadow mask. The voltage sweeps are driven manually with a Tektronix PWS4721 power supply (15 V max) until luminescence is observed by the CCD-camera under microscopy. Due to the lack of sealing of the device, the sweeps are performed within a minute until degradation of the EL-sample.

e. Quantum mechanical calculations

Potential energy surface (PES) analyses of the **n-BG** and **p-R** were performed with density functional theory (DFT). Different conformers were studied by rotating both dihedral angles at the oxygens in 9 steps of 20° with the corresponding geometry optimization at each point (relaxed PES scan). The hybrid density functional method B3LYP was employed in conjunction with the double basis set (6-31G) using the Gaussian 09 software. All the calculations were carried out considering the solvent effect (*n*-butanol or DMSO) by means of the Polarizable Continuum Model (PCM) using the integral equation formalism variant (IEFPCM), default of the SCRF (self-consistent reaction file) method. The charge density was simulated by the CHelpG method, which fits the charge of each atom to the molecular electrostatic potential.

IV. Supporting figures and tables

Table S1: Photophysical properties of **n-BG** and **p-R** in solution (1.0×10^{-5} M). k_r is determined experimentally using the relations $\Phi_{em} = k_r\tau = k_r/(k_r + k_{nr})$. k_r^{calc} is calculated using the Strickler-Berg relation (see below).

	λ_{abs}^{0-0} (nm)	ε (10^4 $M^{-1}cm^{-1}$)	λ_{em} (nm)	Φ_{em}	τ (ns)	k_r (10^7 s^{-1})
n-BG cyclohexane	428		435	0.32[a]	6.03	5.3
n-BG THF	430	1.78 (@404 nm)	449/475	0.29[a]	6.5	4.5
n-BG acetone	430		462	0.26[a]	[b]	[b]
p-R toluene	573	2.6 (@573 nm)	603	0.73[a]	8.3	8.8
p-R cyclohexane	567	2.65 (@567 nm)	599	0.76[c]	9.2	8.2 / 8.42[calc]

a: reference 9,10-diphenylanthracene in cyclohexane (Φ=0.90), λ_{ex} = 402 nm; b: see Table below; c: ref. Sulforhodamine 101 in ethanol (Φ=0.95).

Table S2: Quantum yield Φ_{em} and decay times τ of **n-BG** in solution (mono- or bi-exponential fitting $\Sigma A_i e^{-t/\tau_i}$) in different solvents *vs.* solvent polarity (Δf derived from the Mataga scale, see below).

Solvent	Δf	Φ_{em}[a]	Rel. Amp. A_1	τ_1 (ns)	Rel. Amp. A_2	τ_2 (ns)	kr_1[b] ($\times10^7 s^{-1}$)
cyclohexane	0	0.32	--	6.0	--	--	5.3
diethylether	0.17	0.26	0.91	6.6	0.09	2.5	3.9
Ethyl acetate	0.20	0.28	0.92	6.4	0.08	2.5	4.4
i-propanol	0.28	0.35	0.88	6.8	0.12	2.6	5.1
acetone	0.28	0.26	0.92	6.2	0.08	2.5	4.2
ethanol	0.29	0.35	0.86	6.6	0.14	2.4	5.3
acetonitrile	0.31	0.35	0.86	6.6	0.14	2.5	5.3

a: reference 9,10-diphenylanthracene (DPA) in THF, λ_{ex} = 402 nm; b: radiative constant calculated using Φ_{em} and τ_1.

Equations 1:

$$Strickler-Berg:\ k_r = \frac{1}{\tau_0} = 2.880\times10^{-9}\times n^2\times\frac{\int I(\bar{\upsilon})d\bar{\upsilon}}{\int \bar{\upsilon}^{-3}I(\bar{\upsilon})d\bar{\upsilon}}\times\int \epsilon\, dln\bar{\upsilon}$$

$$Lippert-Mataga:\ \Delta f = [(\varepsilon-1)/(2\varepsilon+1)] - [(n^2-1)/(2n^2+1)]$$

$$\Sigma_f = [(\varepsilon-1)/(2\varepsilon+1)] + [(n^2-1)/(2n^2+1)]$$

$$(\mu_e-\mu_g) = \sqrt{slope1\times\frac{hca^3}{2}} \qquad \mu_g = \frac{-slope2-slope1}{2}\sqrt{\frac{hca^3}{2\times slope1}}$$

$$linear\ regression\ of\ (\bar{\nu}_{abs}-\bar{\nu}_{em})\ vs.\Delta f : slope1; \quad lin.regr.of\ (\bar{\nu}_{abs}+\bar{\nu}_{em})\ vs.\Sigma_f : slope2$$

Where: *For Strickler-Berg:* ϵ is the extinction coefficient in $M^{-1}cm^{-1}$, $\bar{\upsilon}$ are the wavenumbers in cm^{-1}, I is the emission intensity. The degeneracy factor was set to 1. This version of the Strickler-Berg equation is valid for molecules, and in particular in which the absorption and emission imply the same excited state (such as in fully dissolved molecules).
For *Lippert-Mataga:* ε is the dielectric constant and n is the refractive index of the solvent; μ_g and μ_e are the dipole moments in the ground and excited state, respectively; h is the Planck constant; c is the speed of light. The cavity radius of the molecule, a, was determined by matching μ_g calculated with these spectroscopic data and the dipole moment calculated theoretically for the most stable conformer (see below).

Results of the analysis resulting from equations 1 and Figures S1:
a = 7 Å (*for* μ_g = 1.9 D)
μ_e = 14.1 D (*with* μ_g = 1.9 D and a = 7 Å)

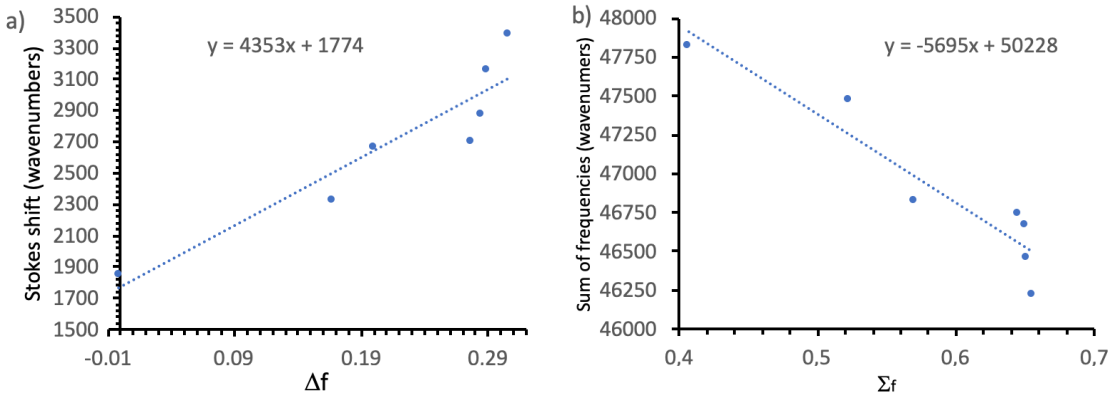

Figure S1: Spectral data (in cm^{-1}) of **n-BG** (1.0×10^{-5} M) in different solvents analysed according to the Lippert-Mataga theory (see equations above). a) Stokes shifts ($\bar{\nu}_{abs} - \bar{\nu}_{em}$) *vs.* Δf, inset: linear regression yields *slope1* = 4353; b) frequency sum $\bar{\nu}_{abs} + \bar{\nu}_{em}$ *vs.* Σ_f, inset: linear regression yields *slope2* = -5695.

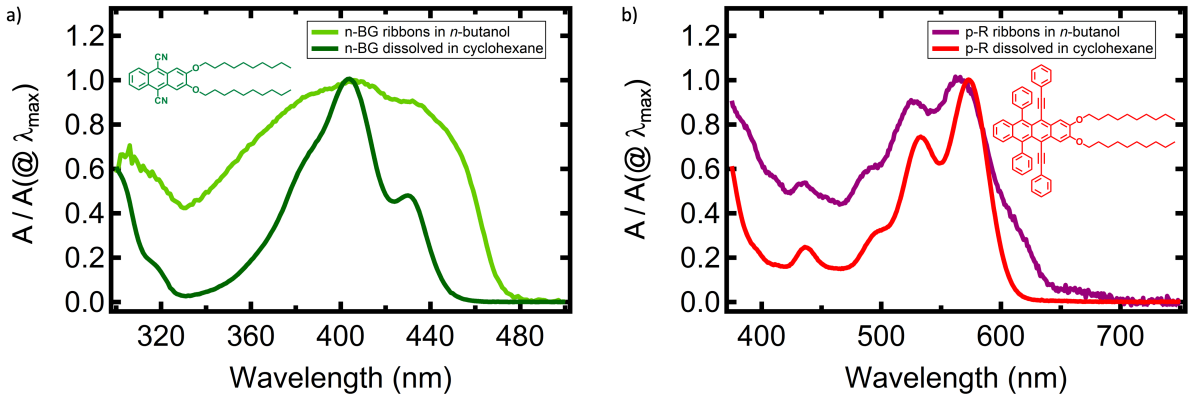

Figure S2: Relative absorption spectra A/A(@λ_{max}) in solution and in pristine ribbons (the latter obtained by synchronous scan, see experimental): a) **n-BG** dissolved in cyclohexane and **n-BG** ribbons formed in *n*-butanol. b) **p-R** dissolved in cyclohexane and **p-R**-ribbons formed in *n*-butanol.

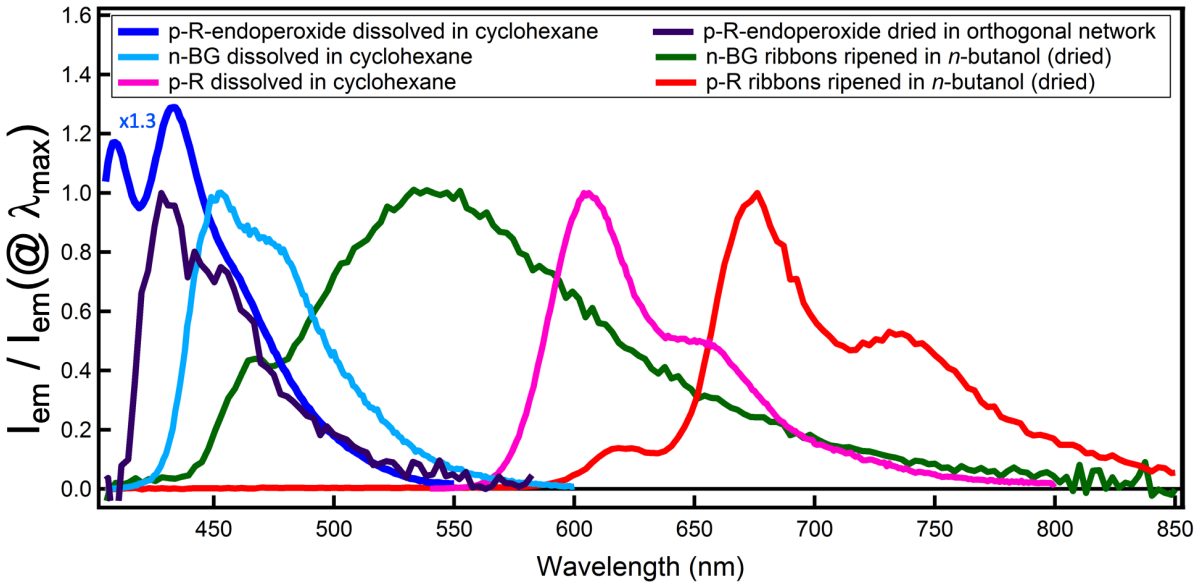

Figure S3: Relative emission intensity spectra $I_{em}/I_{em}(@\ \lambda_{max})$ of **n-BG** and **p-R** dissolved in cyclohexane, and nanoribbons of **n-BG** and **p-R** formed in *n*-butanol. The spectrum of photo-oxidized **p-R** dissolved and in ribbons is also shown (a factor 1.3 was applied for Figure clarity).

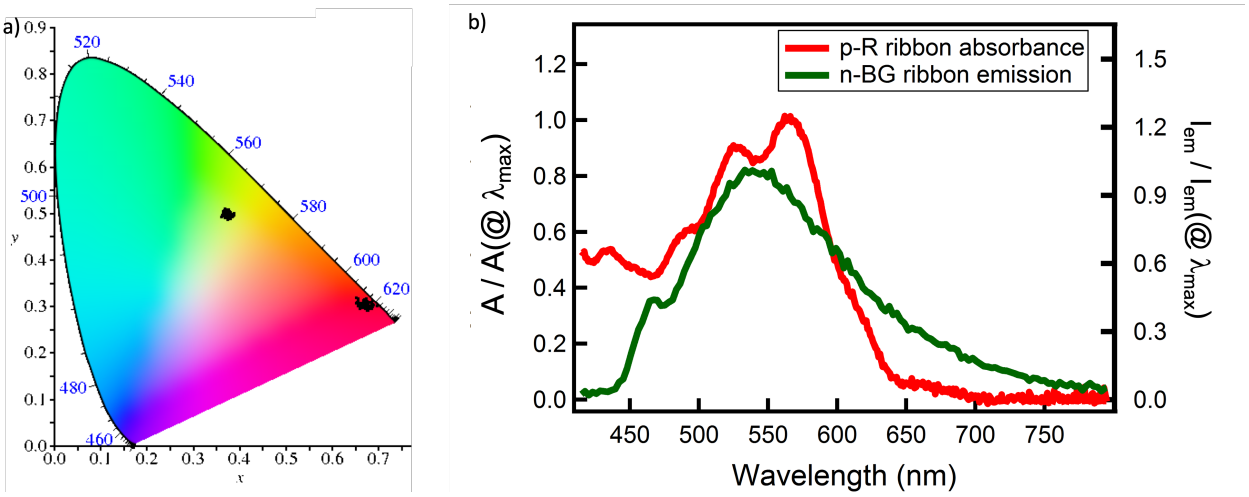

Figure S4: a) CIE-coordinates distribution of the emission of nanoribbons of **n-BG** and **p-R** formed in *n*-butanol: each point corresponds to one pixel in the hyperspectral fluorescence microscopy image shown in the main manuscript. b) Overlap of the relative absorption spectrum of **p-R** ribbons and relative emission spectrum of **n-BG** ribbons, a requisite for FRET energy transfer.

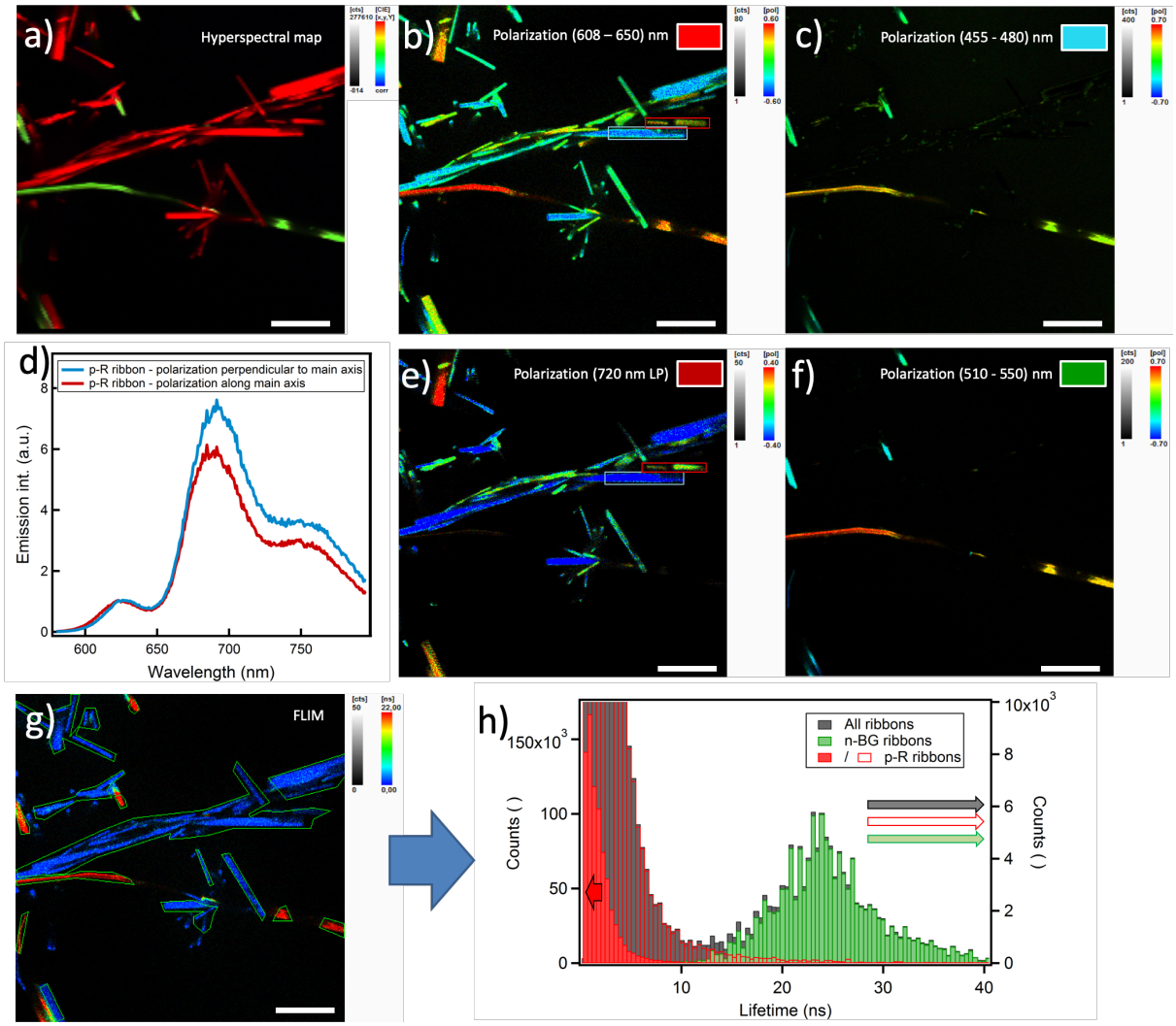

Figure S5: a) Hyperspectral image of **n-BG** and **p-R** ribbons simultaneously in pure *n*-butanol. b) Polarization image with bandpass filter (608 – 650) nm of the emission of the first band of **p-R**: wide ribbons show highly polarized emission which is oriented perpendicular to the long axis of the ribbons; some less wide ribbons show a different polarization (red rectangle ROI). c) Polarization image with bandpass filter (455 - 480) nm adapted to **n-BG** emission: the emission is highly polarized and oriented along the long axis of the ribbons. d) Polarization-resolved fluorescence spectra of two ribbons highlighted in images *b* and *e* with rectangular ROIs: the spectra are normalized at 620 nm and differences are observed at higher wavelengths (no G-factor was applied, thus spectra could be affected by instrumental response). e) Polarization image with longpass filter (720 nm) of the emission of **p-R** ribbons; the wider ribbons show high polarization, whereas some ribbons show no polarization (could be lying on their edge). f) Polarization image with bandpass filter (510 - 550 nm) adapted to **n-BG** excimer emission: the emission is very highly polarized and oriented along the long axis of the ribbons. g) fluorescence (average) lifetime image of the same field of view. Scale bars: 10 µm. h) Corresponding histogram of average fluorescence lifetimes of all pixels (in g, black bars), of selected red-emissive ribbons (red bars) and of selected green-emissive ribbons (green bars) showing well separated lifetime distributions $\tau_{\mathbf{p\text{-}R}} = (0.9 \pm 0.7)$ ns, $\tau_{\mathbf{n\text{-}BG}} = (23.6 \pm 6.2)$ ns.

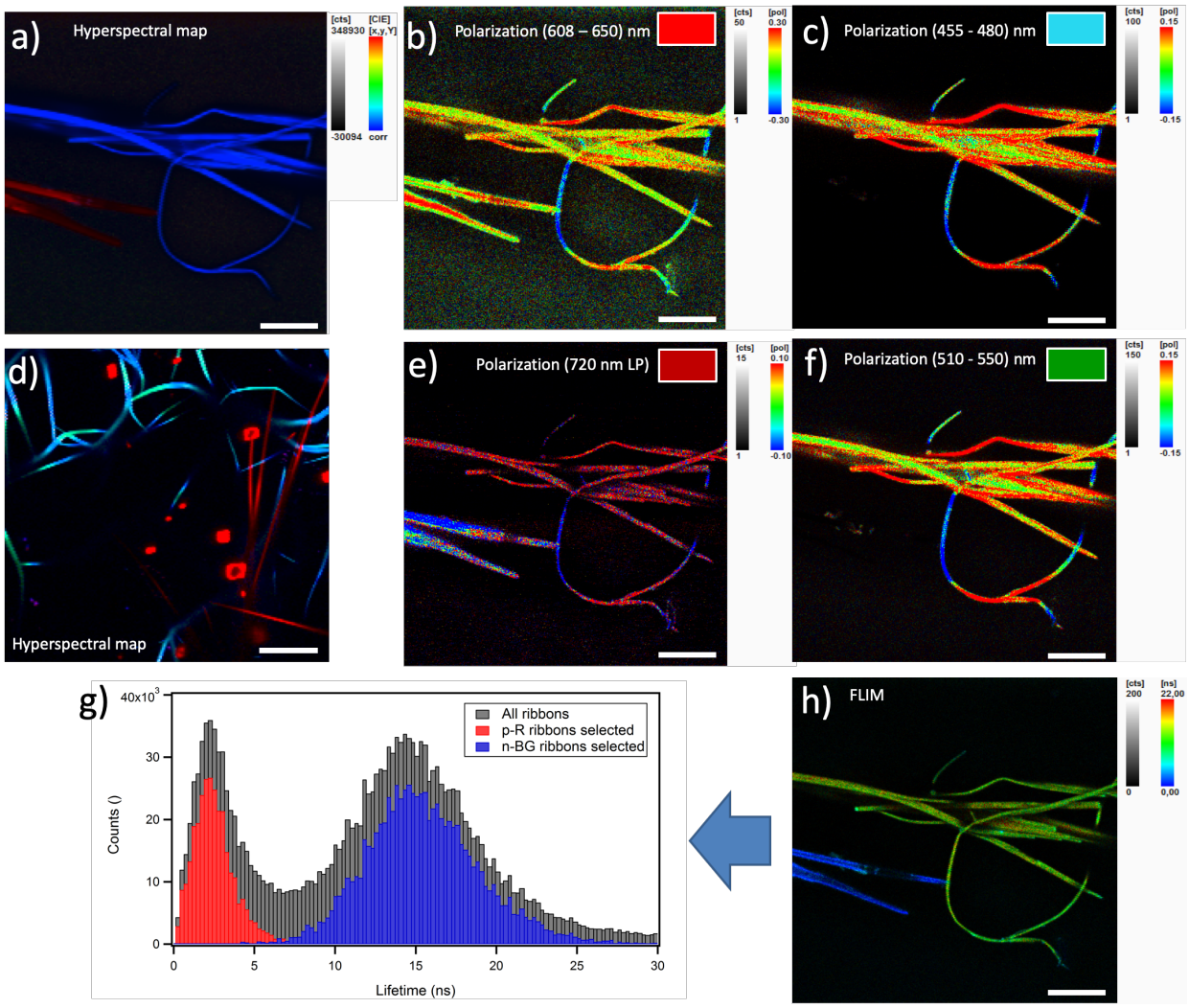

Figure S6: a) Hyperspectral image of **n-BG** and **p-R** ribbons simultaneously in pure DMSO. b) Polarization image with bandpass filter (608 – 650) nm of the emission of the first band of **p-R**: emission is oriented strongly along the long axis of the ribbons; edges can show lower polarization. c) Polarization image with bandpass filter (455 - 480) nm adapted to **n-BG** emission: the emission is oriented along the long axis of the ribbons, but with low P. d) Hyperspectral image of nanoribbons in DMSO (not dried). The lack of confinement of samples in z leads to an artefact in slightly off-focus **n-BG**-ribbons, attributed to the cutting the blue edge of the spectrum by the pinhole. Rectangular features correspond to vertically grown **p-R** structures. e) Polarization image with longpass filter (720 nm) of the red-shifted emission of **n-BG** and **p-R** ribbons: for **p-R** the emission is slightly polarized and perpendicular to the long axis of the ribbons; for **n-BG** the emission is mainly oriented along the long axis of the ribbons. f) Polarization image with bandpass filter (510 - 550 nm) adapted to **n-BG** ribbons: similar to the (455 - 480) nm case. g) Histogram of average fluorescence lifetimes of all pixels (in h)) (black empty bars), of selected red-emissive ribbons (red bars) and of selected blue-emissive ribbons (blue bars) showing well separated lifetime distributions $\tau_{p\text{-}R}$ = (2.1 ± 1.5) ns, $\tau_{n\text{-}BG}$= (15.0 ± 4.6) ns. h) Corresponding fluorescence (average) lifetime image of the same field of view. Scale bars: 10 µm. *Note Figure d:* The hyperspectral image

shows **p-R**-ribbons with rectangular cross-section and some with non-emissive center parts. Either the center is hollow, or the emission of the molecules in the center is suppressed by an inner-filter effect or a quenching process. In a series of hyperspectral images (z-stacks, not shown), the center becomes emissive like the edges a bit further away from the glass surface. One possibility is that non-emissive centers are constituted by the seeds which form first at the glass surface and then support the growth of the ribbons.

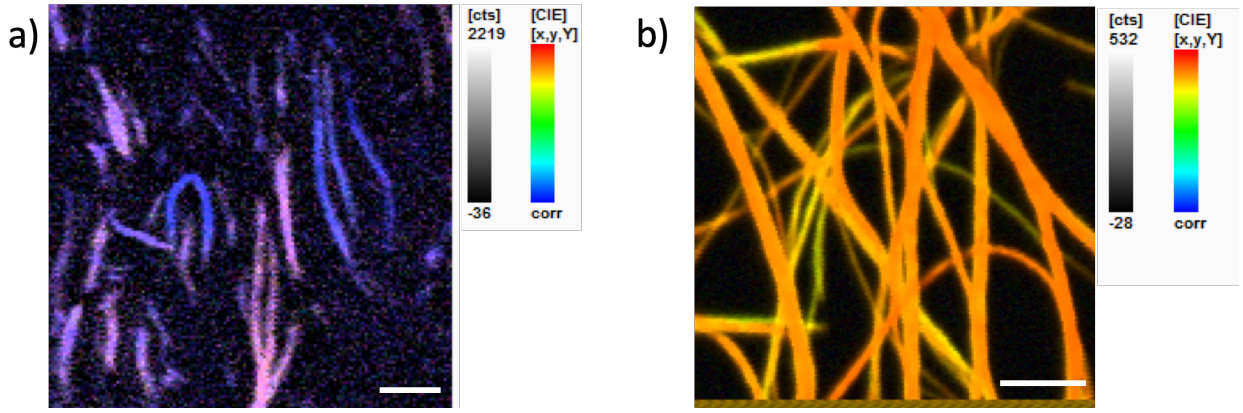

Figure S7: a) Hyperspectral image of **p-R** mixed with 2,3-didecyloxyanthracene (DDOA) in DMSO: no red-emitting pure **p-R** ribbons are observed (most nanoobjects emit pink/purple light from mixed objects, and some blue like pure DDOA). Scale bar is 3 µm. b) Hyperspectral image of **p-R** mixed with 2,3-didecyloxy-9,10-diphenylethynyl-anthracene (DDPEA) in DMSO: no red-emitting pure **p-R** ribbons are observed (most nanoobjects emit orange light from mixed objects). Scale bar is 3 µm. Areas shown in a) and b) are representative, but samples are not homogeneous.

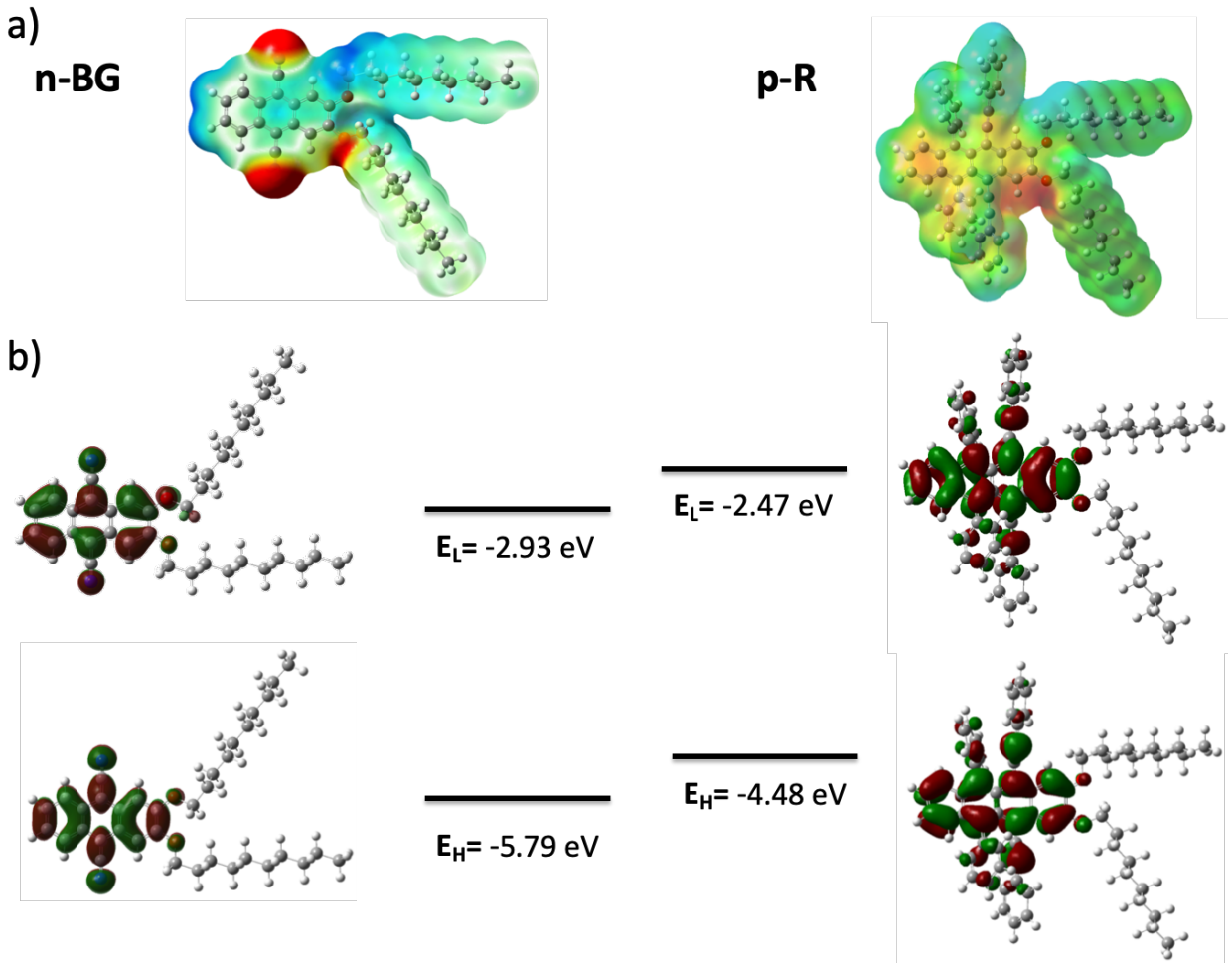

Figure S8: a) Calculated charge density of **n-BG** and **p-R** in *n*-butanol solution of meta-stable asymmetric conformers, obtained by energy minimization upon rotation of the C(ar)-O-C-C(alk) torsional angle. Both molecules display a large dipolar moment of 4.11 Debye for **n-BG** and 3.46 Debye for **p-R**. b) Calculated HOMO and LUMO orbitals of **n-BG** and **p-R** in *n*-butanol solution of meta-stable asymmetric conformers.

Table S3: Calculated dipoles and energies of the most stable symmetric conformer and the meta-stable asymmetric conformer of **n-BG** and **p-R** in different solvents. Mol% of different conformers are calculated according to a Boltzmann distribution using the energies calculated.

n-BG	THF		Butanol			DMSO		
	μ_{THF} (Debye)	Energy (Hartree)	$\mu_{Butanol}$ (Debye)	Energy (Hartree)	mol% at 373 K	μ_{DMSO} (Debye)	Energy (Hartree)	mol% at 373 K
Symmetric	2.00	-1660.297	1.93	-1660.299	98.4	1.88	-1660.300	98.4
Asymmetric	3.99	-1660.292	4.11	-1660.294	1.6	4.18	-1660.295	1.6

p-R	THF		Butanol			DMSO		
	μ_{THF} (Debye)	Energy (Hartree)	$\mu_{Butanol}$ (Debye)	Energy (Hartree)	mol% at 373 K	μ_{DMSO} (Debye)	Energy (Hartree)	mol% at 373 K
Symmetric	1.25	-2705.736	1.22	-2705.739	97.5	1.19	-2705.740	97.8
Asymmetric	3.34	-2705.732	3.46	-2705.734	2.5	3.56	-2705.736	2.2

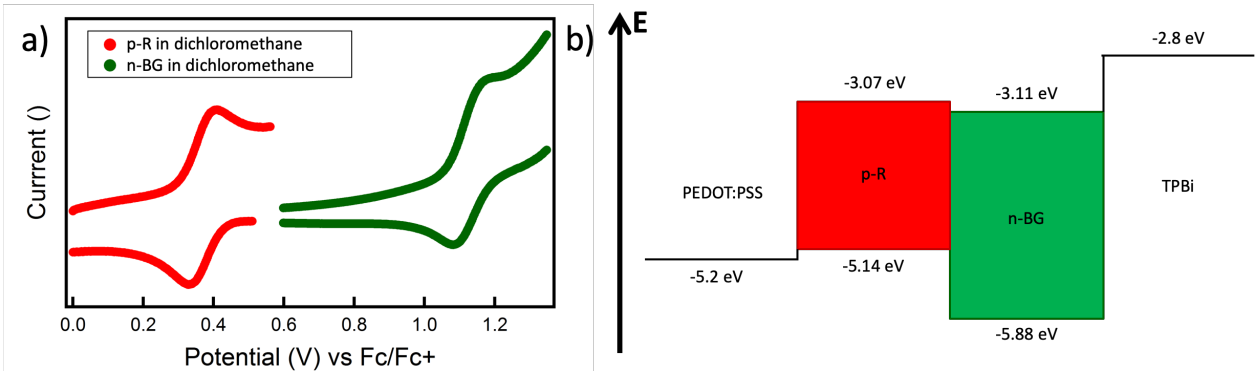

Figure S9: a) Cyclic voltammetry of the oxidation (HOMO) of **p-R** (red) and **n-BG** (green) in dichloromethane. b) Bandstructure for an electroluminescent crossing of **p-R** ribbon and **n-BG** ribbon, with HOMO and LUMO levels estimated from cyclic voltammetry and the bandgap derived from the absorption edge of the compounds.

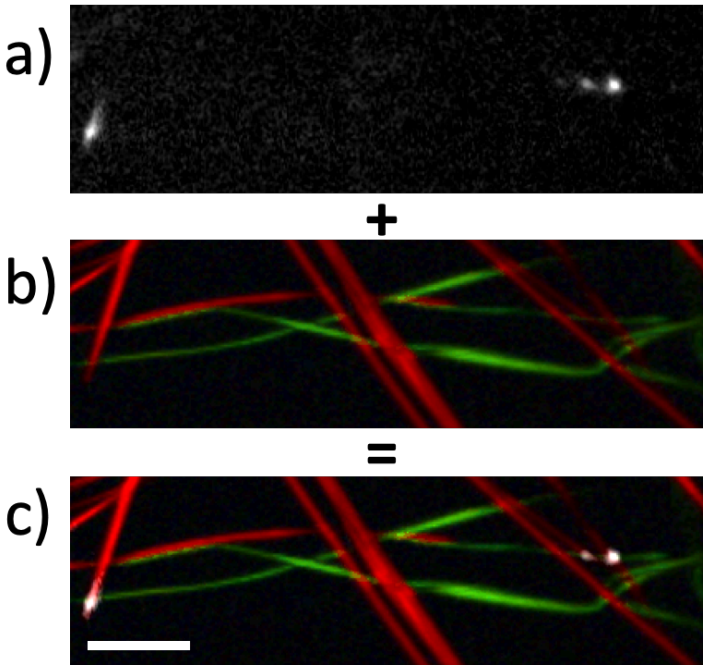

Figure S10: Electroluminescent device of **n-BG** and **p-R** ribbons: a) Electroluminescence image recorded using the CCD-camera, integrated over a voltage sweep up to 10 V. b) Subsequent fluorescence hyperspectral image acquired by confocal microscopy of the same sample area. c) Overlay of the electroluminescence image and the hyperspectral image. (Scale bar: 10 µm)

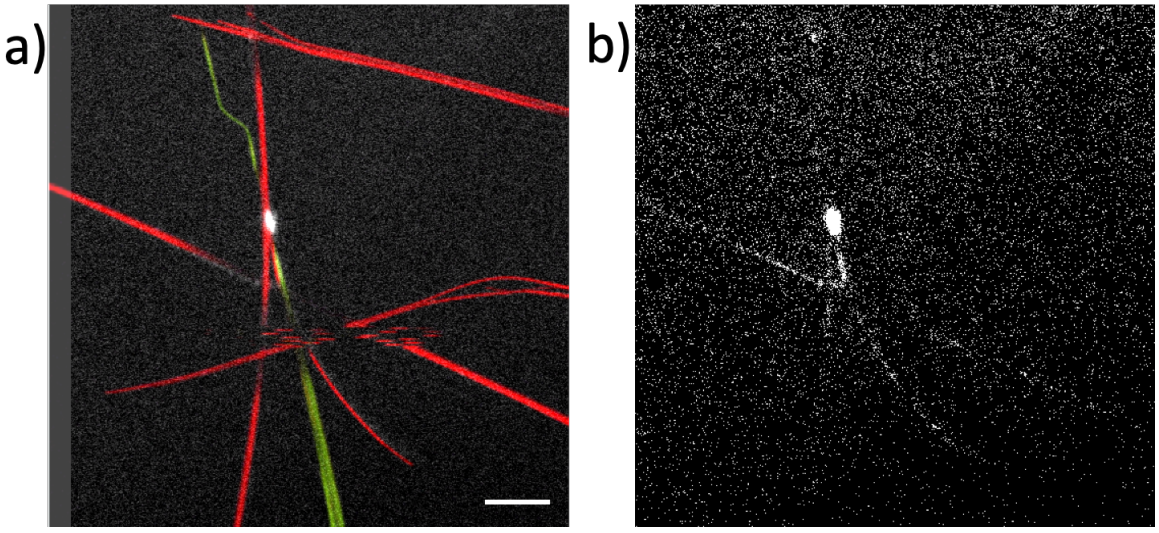

Figure S11: a) Overlay of electroluminescence and hyperspectral images of **n-BG** and **p-R** ribbons (similar to Figure S9). b) Electroluminescence image of the same with a different intensity scale revealing the weak EL from **p-R** outside of junctions. (Scale bar: 10 µm)